Comparison of theoretical and experimental electronic distributions of Si - Ni and Si - Er alloys

1996 J. Phys.: Condens. Matter 8 719

(http://iopscience.iop.org/0953-8984/8/6/012)

J. Phys.: Condens. Matter **8** (1996) 719–728. Printed in the UK

Comparison of theoretical and experimental electronic distributions of Si–Ni and Si–Er alloys

A Gheorghiu†, C Sénémaud†, E Belin-Ferré†, Z Dankhàzi†‡,
L Magaud-Martinage§ and D A Papaconstantopoulos‖

† Laboratoire de Chimie Physique Matière et Rayonnement, Unité de Recherche associée au CNRS 176, 11 rue Pierre et Marie Curie, 75231 Paris Cédex 05, France

‡ Institute for Solid State Physics, Eötvös University, Muzeum krt 6-8, 1088 Budapest, Hungary

§ Laboratoire d'Etudes des Propiétés Electroniques des Solides CNRS, 25 avenue des Martyrs, BP 166X, 38042 Grenoble, France

‖ Naval Research Laboratory, Department of the Navy, Code 4690, Washington, DC 20375-5000, USA

Received 26 June 1995, in final form 6 October 1995

Abstract. The total and partial densities of states of $SiNi_3$, Si_2Ni and $Si_{1.7}Y$ have been calculated using a scalar relativistic self-consistent augmented plane-wave method ($SiNi_3$) or a self-consistent linear muffin-tin orbital method in the atomic sphere approximation (Si_2Ni and $Si_{1.7}Y$). The x-ray photoemission valence band and soft-x-ray emission Si Kβ and Ni Lα spectra have been calculated by applying appropriate broadening factors to the theoretical densities-of-states curves; in the case of the x-ray photoemission spectra, photoionization cross sections have been taken into account. Very good agreement is found between the experimental x-ray photoemission and soft-x-ray emission spectra and the simulated spectral curves.

1. Introduction

Transition-metal and rare-earth (RE) silicides are materials that have possible applications in microelectronics industry. They can be obtained in a wide variety of crystalline as well as amorphous structures. Many of them are chemically stable and resistant to corrosion and aging. Thus, most attention is paid to these compounds not only from the experimental point of view but also because there is interest in the theoretical examination of their electronic properties. Indeed, knowledge of the electronic structure is necessary to understand the physical and electronic properties.

The electronic states of the valence band (VB) of a solid can be studied using both x-ray photoelectron spectroscopy (XPS) and soft-x-ray emission spectroscopy (SXES). These are complementary techniques; indeed, by XPS, the total VB distribution, modulated by photoionization cross sections, is obtained whereas, using XES, the partial and local VB densities of states (DOS) are analysed. In the case of amorphous Si–Ni alloys, such XPS and SXES investigations showed that the Si 3p distribution is considerably modified as x increases from 0 to 0.71 and its maximum is pulled down to higher binding energies. At the top of the VB, Si 3p states are progressively replaced by Ni 3d states which are responsible for the metallic character of the alloy with $x = 0.71$ (Gheorghiu *et al* 1995). A similar result was obtained previously for Si_2Co from the experimental analysis of Si 3p and Co 3d VB states; in this case, excellent agreement was also found between experimental data

0953-8984/96/060719+10$19.50

and theoretical calculations using a scalar relativistic self-consistent augmented plane-wave calculation (Belin *et al* 1990).

The purpose of this work is to analyse by theoretical as well as by experimental means the VB DOSs for several silicides. Since it is known that the gross features of the DOSs mainly arise from the local order, i.e. the chemical bond, to test the validity of the theoretical methods, we have compared in the following the results of DOS calculations, which are available only for several ordered systems, to the experimental data obtained from amorphous alloys of nearby nominal composition.

Previous experimental SXES investigations on pure Si have shown that no significant modifications due to H can be detected in the Si 3p spectral distributions; only the VB edge is slightly shifted towards high binding energies in amorphous hydrogenated Si with respect to amorphous Si (Sénémaud *et al* 1982).

In section 2 of this paper, we report the DOS calculations for crystalline $SiNi_3$, Si_2Ni and $Si_{1.7}Y$. This last compound has been shown to be representative of the RE disilicide family (Magaud *et al* 1992b). The experimental investigation of the VB electronic distributions was performed on amorphous Si–Ni alloys of nominal composition close to that of the crystalline alloys and on crystalline $Si_{1.7}Er$. The total VB distribution was obtained from XPS; the Si 3p states of both Si–Ni and Er–Si alloys as well as Ni 3d states for Si–Ni were obtained from SXES measurements. The corresponding results are given in section 3. Section 4 is devoted to a discussion of the results and a comparison between experiments and calculations.

2. Calculations

$SiNi_3$ and Si_2Ni crystallize in the cubic Cu_3Au and fluorite structures, respectively. In $SiNi_3$, the lattice parameter of the elemental cube is $a_0 = 0.3507$ nm; the structure is close packed similar to that of pure Ni, but here Si atoms are at the corners of the elemental cube. In Si_2Ni, the FCC lattice parameter is $a_0 = 0.5395$ nm; the lattice consists of a simple-cubic array of Si atoms with the Ni atom, which belongs to another cube, located at its centre (Martinage *et al* 1990).

All trivalent RE disilicides crystallize in a hexagonal lattice of the AlB_2 type with silicon vacancies. This results in a $Si_{1.7}RE$ stoichiometry. The surface shows a $(\sqrt{3} \times \sqrt{3})$ R(30) reconstruction which is assumed to extend in the bulk (Baptist *et al* 1990). The vacancies induce a relaxation and the structure is equivalent to the Si_5Yb_3 structure. We used the experimental atomic positions as determined by Iandelli *et al* (1979) scaled to the $Si_{1.7}Y$ lattice parameters $a = 0.3842$ nm and $c = 0.414$ nm. This structure has been described in detail elsewhere (Magaud *et al* 1992a).

In a previous calculation (Magaud *et al* 1992b) it has been emphasized that nearly identical DOSs are obtained for Si_2Y and Si_2E although Y has no f electrons. This is not surprising because all trivalent RE disilicides and Si_2Y share the same crystallographic structure and the same electronic configuration if we exclude the f electrons so that, although Y has no f electron, it is assumed to be similar to a RE element. Let us recall that, furthermore, 4f electrons have been shown experimentally to play a minor role as far as the electronic structure is concerned (Veuillen *et al* 1991a, b). $Si_{1.7}Y$ is then representative of the $Si_{1.7}RE$ family. The absence of f electrons facilitates the use of our linear muffin-tin orbitals (LMTO) code and allows the treatment of vacancies. We could have performed a $Si_{1.7}Er$ calculation with f states in the core; however, our previous work (Magaud *et al* 1992b) suggests that this is not necessary.

Our band-structure calculations were performed by the augmented plane-wave (APW)

method for $SiNi_3$ and by the LMTO method for Si_2Ni and Si_2Y. The two methods give nearly identical results and the choice of different methodologies for the particular compound is a matter of convenience for the different collaborators of this work. In both methods we used the local-density approximation formulation of Hedin and Lundqvist (1971) to treat exchange and correlation. In the APW calculations we used a scalar relativistic code in the muffin-tin approximation. This was an all-electron calculation treating the inner electrons as atomic like and the outer electrons as band like. The calculation of the DOS was done by the tetrahedron method, and comparison with experiment was made after appropriately broadening the partial DOSs as discussed below.

The LMTO calculations were also scalar relativistic but they invoked the frozen-core approximation. Basis functions included angular momentum expansions up to $l = 2$. The k-point convergence was carefully checked and included 180 and 72 k-points in the irreducible Brillouin zone for Si_2Y and Si_2Ni, respectively. We used atomic sphere radii of 0.1836 nm and 0.1534 nm for Y and Si in Si_2Y while the radii were kept equal in the Si_2Ni calculation.

The Fermi level was found to lie in the gap, almost at the minimum of the total DOS, for $SiNi_3$ and close to a pseudo-gap in Si_2Ni.

Examination of the partial DOSs in $SiNi_3$ (figure 1) shows the following.

(i) Si s states are in the higher-binding-energy part of the VB.

(ii) Si p states hybridize with s states mostly between 5 and 8 eV from E_F and slightly interact with Ni d states over about 4 eV from E_F; thus almost Si p pure states are present in a narrow energy range centred at $E_F - 4$ eV.

(iii) The maximum intensity of the Ni 3d quasi-pure states is about 1 eV from E_F.

The maximum intensity of the Ni d states is 23.3 states eV^{-1} in the unit cell. Since the maximum intensities of the Si p states and the Si s states are 2.11 states eV^{-1} and 0.4 states eV^{-1}, respectively, i.e. 11 and 60 times lower, the Ni d states are dominant in the VB.

In Si_2Ni, the maximum of the Ni d states (7.8 states eV^{-1}) is set at about 4 eV from E_F (figure 2). The respective maximum intensities of the Ni s and p states are 0.1_6 states eV^{-1} and 0.2_4 states eV^{-1}, i.e. about 50 and 30 times smaller than that of the Ni d states; thus, one expects these states to contribute insignificantly to the VB. At about 4 eV from E_F the Ni states overlap Si p states. In the highest bonded part of the VB, Si p states hybridize with Si s states so that there are almost no pure Si p states in this alloy. The maximum intensity of the Si p states is 1.3 states eV^{-1} (figure 2). Consequently, for this alloy the Ni d states are dominant in the structure (see upper panels of figure 2).

In $Si_{1.7}Y$ (figure 3), the Y d states exhibit a peak at about 2.5 eV from E_F whose intensity is 2.6 states eV^{-1}. The maximum intensities of the Y s and p states are 0.5 states eV^{-1} and 1.4 states eV^{-1}, respectively. At about 2.5 eV from E_F the Y d states overlap Si p states. The respective maximum intensities of the Si s, p and d occupied states are 2.4 states eV^{-1}, 4.9 states eV^{-1} and 0.5 states eV^{-1}. Thus, hybridized Y p–d states in interaction with Si p states dominate the total VB DOS and are centred around 4 eV from E_F. As for the other silicides, the lowest part of the VB is mostly Si s in character.

3. Experimental procedures

As already mentioned above, the samples which we have investigated were amorphous Si–Ni:H alloys of nominal composition close to that of the crystalline $SiNi_3$ and Si_2Ni alloys and crystalline $Si_{1.7}Er$. Details concerning the sample preparation procedures have been given elsewhere (Magaud *et al* 1992a, b, Gheorghiu *et al* 1995). Let us recall that

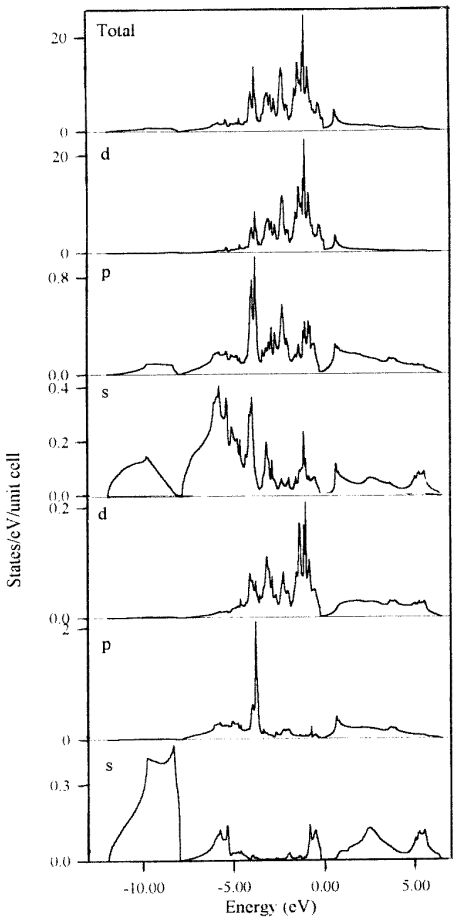

Figure 1. Calculated DOSs for Ni_3Si: from bottom to top, partial Si s, p and d Si DOSs, partial s, p and d DOSs and total Ni_3Si DOS.

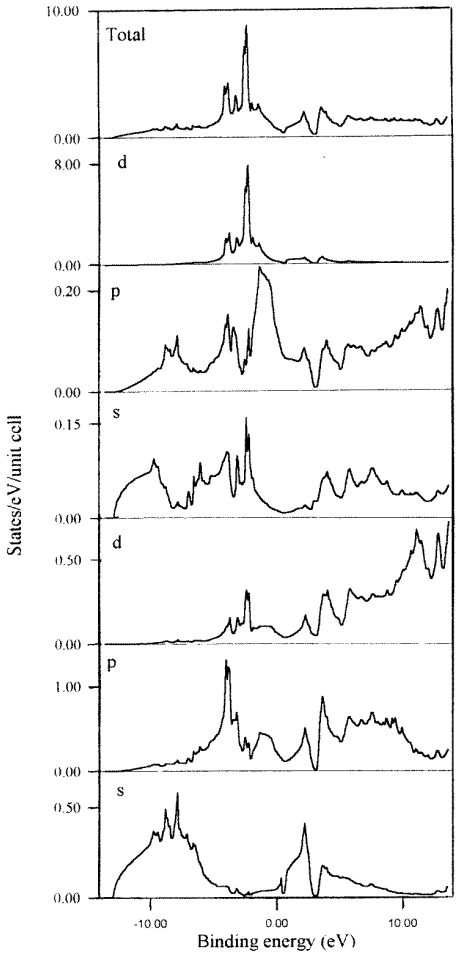

Figure 2. Calculated DOSs for $NiSi_2$: from bottom to top, partial Si s, p and d DOSs, partial Ni s, p and d DOSs and total $NiSi_2$ DOS.

the a-$Si_{1-y}Ni_y$:H samples with $y = 0.35$ and 0.71 were prepared by RF sputtering. The $Si_{1.7}Er$ alloy thin films were epitaxially grown onto Si(111) crystals by first evaporating an Er layer onto a clean Si(111) surface and then depositing a Si capping layer onto the Er layer (Magaud *et al* 1992a, b). Anneals at 800–850 °C for 5–10 min were performed in order to induce the chemical reaction. The formation of the sample was controlled by the observation of the characteristic $(\sqrt{3} \times \sqrt{3})$ R(30) low-energy diffraction pattern (Arnaud d'Avitaya *et al* 1989).

The measurements of the energy distribution of the VB states for the various samples have been performed using both SXES and XPS. In the former case, we measure the intensity of photons emitted during the recombination of an inner hole from the VB; in the second case we measure the kinetic energy of electrons ejected from the VB that is ionized by incoming photons. In SXES, the x-ray transitions are governed by dipole selection

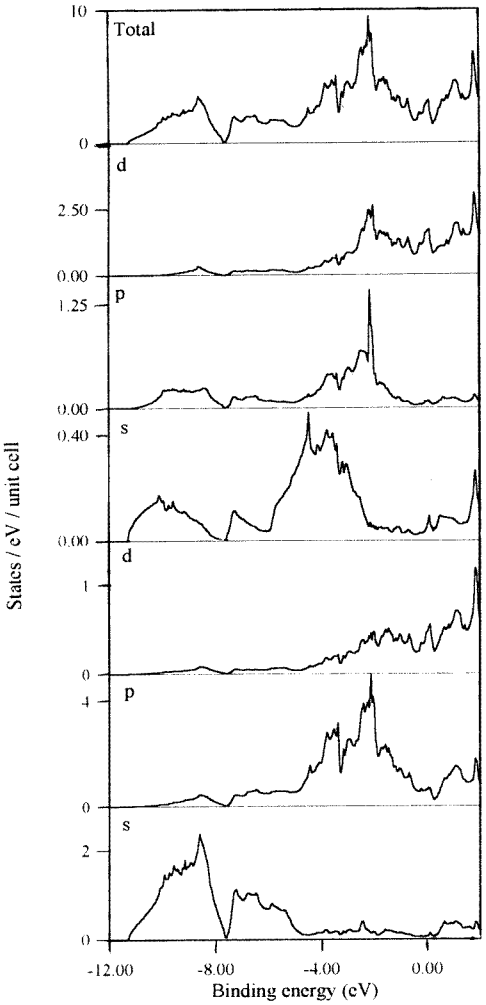

Figure 3. Calculated DOSs for $YSi_{1.7}$: from bottom to top, partial Si s, p and d DOSs, partial Y s, p and d DOSs and total $NiSi_2$ DOS.

rules and are transition probability dependent; so partial local electronic distributions can be obtained. In XPS, the various s, p, d, VB electrons are obtained altogether and their respective intensities are modulated by photoelectron cross sections.

In all alloys we have measured the Si Kβ emission that corresponds to VB $\rightarrow$ Si 1s transitions and thus provides the distribution of Si 3p states. For the Ni–Si alloys we have also measured the Ni Lα emission that corresponds to VB $\rightarrow$ Ni $2p_{3/2}$ transitions and provides the Ni 3d distribution. For such experiments we used Johann-type bent-crystal vacuum spectrometers fixed with a $SiO_2(10\bar{1}0)$ (2d = 850.766 nm) crystal for the Si Kβ emission and a beryl ($10\bar{1}0$) crystal (2d = 1588.52 nm) for the Ni Lα emission. The experimental resolutions are about 0.3 eV in each case. The x-ray photoelectron spectra were obtained with a Kratos spectrometer using incoming Mg Kα radiation. The energy

resolution is about 0.8 eV.

The experimental curves are normalized to their maximum intensity. They are all set to the binding energy scale. For such an adjustment, we have located the Fermi energy on the x-ray transition energy scale of each SXES curve owing to the determination of the binding energy of the core levels involved in the corresponding x-ray transition. This could be achieved from the measurement of the binding energies of Si and Ni $2p_{3/2}$ core levels referenced to the Fermi level and the energy of the Si Kα_1 x-ray emission line (Si $2p_{3/2} \rightarrow$ Si 1s) (Sénémaud and Ardelean 1990).

4. Results and discussion

For a meaningful comparison between calculations and experimental results, we have calculated x-ray and photoemission spectra in the framework of the one-electron picture using the theoretical partial and total DOS results.

For calculating soft-x-ray emission spectra we have convoluted the calculated partial DOS by a Lorentzian distribution $\mathcal{L}$ that accounts for the energy width of the inner level that participates in the x-ray transition (DOS $\times$ $\mathcal{L}$). The energy width is 0.45 eV for Si 1s and 0.5 eV for Ni $2p_{3/2}$ (Keski-Rahkonen and Krause 1974). We have not included transition probabilities because it is known that, as long as one uses a site angular and momentum-decomposed DOS, these may be considered as constant in the whole energy range that refers to the experiments (see also Lerch *et al* (1992)). For calculating the Ni Lα spectrum we have considered only the theoretical d DOS since, as pointed above, the s DOS is negligible with respect to the d DOS; moreover, it should be noted that transition probabilities favour d states compared to s states. In order to account for the broadening due to the experimental function of the spectrometer, we have also convoluted the DOS $\times$ $\mathcal{L}$ result by a Gaussian function G. In all SXES calculations we have used a G distribution with a FWHM of 0.3 eV. For simulating the x-ray photoelectron spectra, we have summed together all the various calculated partial DOSs that contribute to the VB modulated by the corresponding photoemission cross sections (Scoffield 1976). In addition, we have convoluted the result by a convenient G distribution that accounts for the experimental broadening.

Finally, the resulting calculated SXES and XPS curves have been normalized to their maximum intensity taken as the unit. These various 'theoretical' spectra will be compared to the corresponding experimental spectral curves in the following paragraphs.

4.1. a-$Si_{29}Ni_{71}$:H and $SiNi_3$

Experimental results for a-$Si_{29}Ni_{71}$:H and calculated data for $SiNi_3$ are displayed in figure 4. In figure 4(*a*) we show the theoretical Ni 3d DOS curve (lower curve), the Ni Lα SXES calculated curve (middle curve) and the experimental Ni Lα curve (upper part). The partial calculated DOS consists of a set of three peaks that produce three shoulders on the high-binding-energy side of the calculated SXES curve. These features are not resolved on the experimental curve. However, fair agreement is observed between the FWHM of the experimental curve for a-$Si_{29}Ni_{71}$:H which is 2.9 ± 0.1 eV and that of the calculated curve for $SiNi_3$ which is 3.0 ± 0.1 eV.

Figure 4(*b*) displays the theoretical Si 3p DOS for Ni_3Si (lower curve), the corresponding calculated SXES curve (middle curve) and the experimental result (upper curve) for a-$Ni_{71}Si_{29}$:H. The partial DOS curve consists of an intense peak centred about 4 eV from E_F and secondary wide peaks in the energy ranges 1.2–3 eV and 5–7 eV from E_F. To all these features correspond a strong peak and broad structures in the calculated soft-x-ray emission

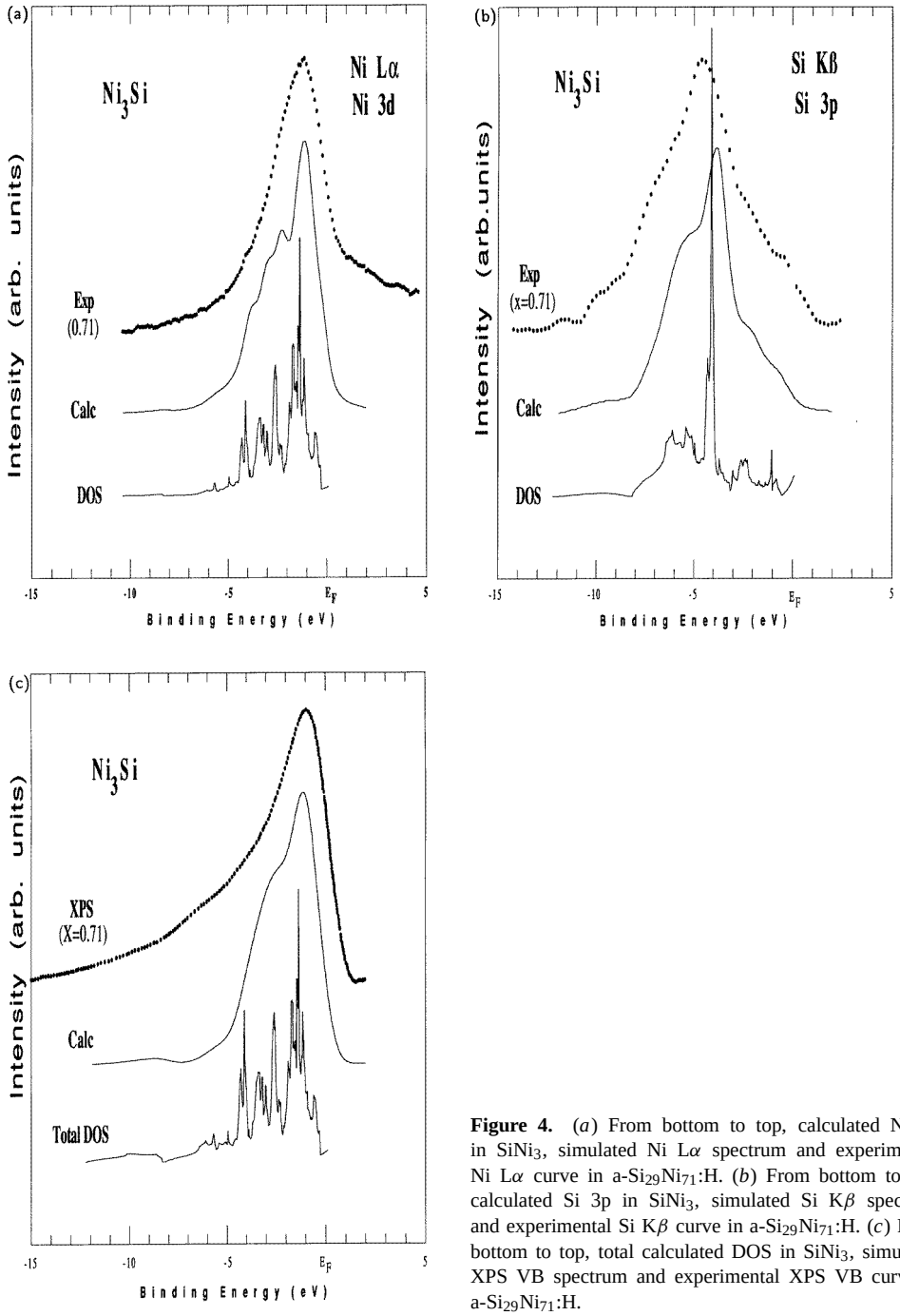

Figure 4. (*a*) From bottom to top, calculated Ni 3d in $SiNi_3$, simulated Ni Lα spectrum and experimental Ni Lα curve in a-$Si_{29}Ni_{71}$:H. (*b*) From bottom to top, calculated Si 3p in $SiNi_3$, simulated Si Kβ spectrum and experimental Si Kβ curve in a-$Si_{29}Ni_{71}$:H. (*c*) From bottom to top, total calculated DOS in $SiNi_3$, simulated XPS VB spectrum and experimental XPS VB curve in a-$Si_{29}Ni_{71}$:H.

spectrum. The experimental curve is in very good agreement with the calculated curve; its maximum reflects Si 3p states in slight interaction with Ni 3d states. Two weak features between E_F and the main peak are due to interacting Si p and Ni d states; their energy positions coincide with those of quasi-pure Ni 3d states. The faint feature on the opposite side from the maximum, at about $E_F - 9.5$ eV, corresponds to hybridized Si 3sp states. Finally, pure Si 3p states are seen as the large shoulder at $E_F - 5.5$ eV.

Figure 4(*c*) presents the theoretical total DOS (lower curve), the calculated total density spectrum as explained above (middle curve) and the experimental x-ray photoelectron spectrum (upper curve). The two sets of peaks of the theoretical DOS that are close to E_F correspond to Ni 3d states and that centred around 4 eV from E_F refers to Ni 3d–Si 3p states. A broad tail that is due to s states is set at around 8–9 eV from E_F. All these features give rise in the calculated spectrum to a single peak with an intense shoulder on the high-binding-energy side and a low broad bump. The shoulder closest to the main peak is not well resolved and is less intense in the experimental curve than in the calculated curve. The high-energy band tail is scarcely seen in the experiment. The FWHMs of the calculated and experimental XPS curves are in fair agreement since they both are 3.7 ± 0.1 eV.

4.2. a-$Si_{65}Ni_{35}$:H and Si_2Ni

The results for a-$Si_{65}Ni_{35}$:H are displayed in figure 5 comparatively to the calculations for Si_2Ni.

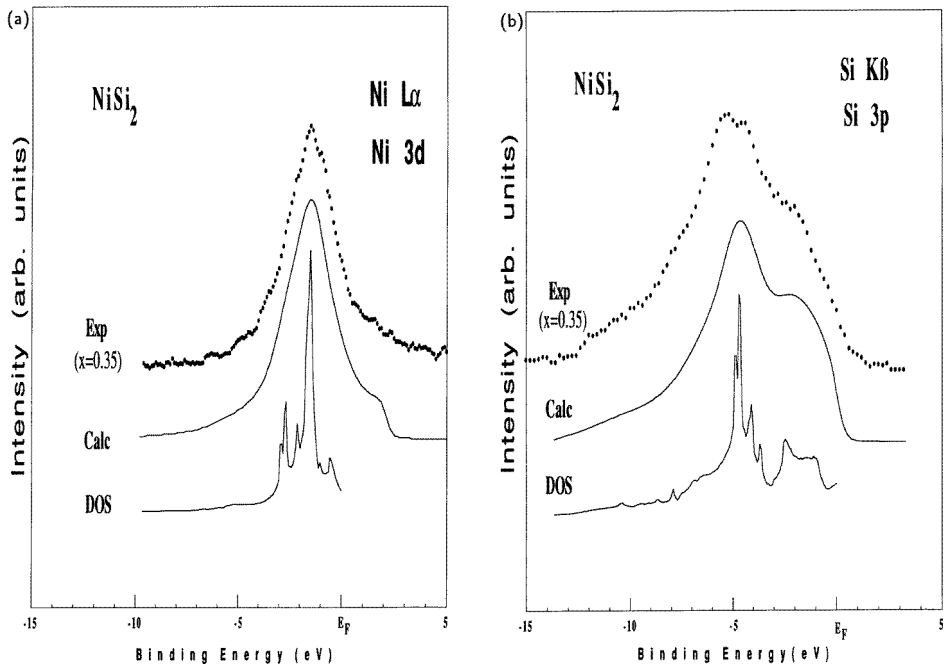

Figure 5. (*a*) From bottom to top, calculated Ni 3d in Si_2Ni, simulated Ni Lα spectrum and experimental Ni Lα curve in a-$Si_{65}Ni_{35}$:H. (*b*) From bottom to top, calculated Si 3p in Si_2Ni, simulated Si Kβ spectrum and experimental Si Kβ curve in a-$Si_{65}Ni_{35}$:H.

In figure 5(*a*) are plotted the theoretical Ni 3d DOS (lower curve) and the calculated Ni Lα SXES curve (middle curve) for $NiSi_2$; the upper curve corresponds to the Ni Lα

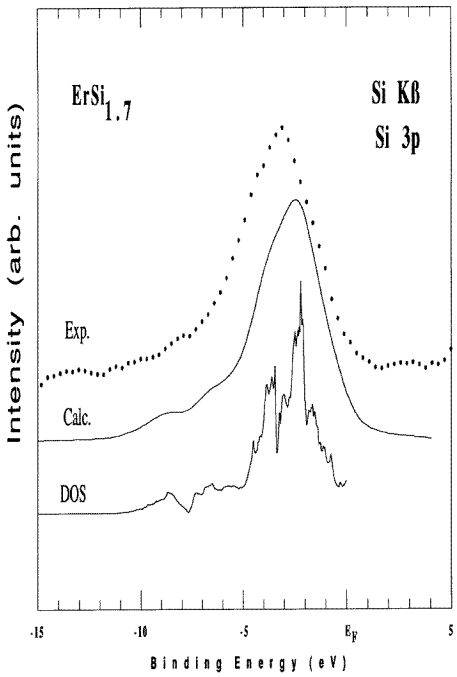

Figure 6. From bottom to top, calculated Si 3p DOS in $Si_{1.7}Y$, simulated Si Kβ spectrum and experimental Si Kβ curve in $Si_{1.7}Er$.

spectrum for a-$Si_{65}Ni_{35}$:H. The partial calculated DOS consists mainly of an intense peak (Ni d non-bonding states) and a faint narrow peak at about 1.5 eV and 3 eV, respectively, from E_F. These peaks are due to Ni 3d states interacting with Si 3p states. They produce a single peak on the calculated SXES curve consistently with the experimental result. The FWHMs of both calculated and experimental curves are about 2.5 ± 0.1 eV in fair agreement.

Figure 5(*b*) shows the calculated Si 3p DOS, the calculated Si Kβ SXES and the experimental Si Kβ curves, and their shapes differ somewhat from those observed for a-$Si_{29}Ni_{71}$:H and $SiNi_3$. On the theoretical DOS curve, two sets of peaks of quite different intensities are centred around 1.5 and 5 eV from E_F. On the calculated spectrum this is seen as two broad peaks. The peak which is closer to E_F is the most intense. Both peaks arise from Si 3p states mixed with Ni 3d states. It should be noted that the positions of the maxima of the calculated and experimental curves are slightly shifted with respect to each other. However, very good agreement is found on adjusting the Si 3p and Ni 3d experimental curves on the binding energy scale since the peak of the curve for the Ni Lα spectrum overlaps the low-energy component of the curve for the Si Kβ spectrum.

4.3. $Si_{1.7}Er$ and $Si_{1.7}Y$

Figure 6 presents the theoretical Si 3p DOS curve and the calculated Si Kβ SXES curve for $Si_{1.7}Y$ (lower and middle curves, respectively); the upper curve corresponds to the experimental Si Kβ spectrum for $ErSi_{1.7}$. The theoretical DOS curve displays roughly a wide set of two peaks. The calculated SXES curve consists of a broad asymmetric peak with two faint bumps towards high binding energies. Thus, the shapes of the experimental

and calculated SXES curves are in good agreement although the FWHMs of these two curves slightly differ; they are 4.0 eV and 3.75 ± 0.1 eV, respectively, for experiment and calculation. A discrepancy is, however, observed. Indeed, the maxima of the experimental and calculated curves do not coincide; the former curve has to be slightly shifted towards E_F to fit the calculated result.

5. Conclusion

The total and partial DOSs of $SiNi_3$, Si_2Ni and $YSi_{1.7}$ have been calculated using scalar relativistic self-consistent APW and LMTO-ASA methods. From these theoretical DOSs, the XPS VB and SXES Si Kβ and Ni Lα spectra have been calculated by applying appropriate broadening factors and taking into account photoionization cross sections in the case of the XPS.

Very good agreement is found between experimental x-ray photoelectron and x-ray emission spectra and the simulated curves with respect to both the peak positions relative to the Fermi level and the overall shape of the electronic distribution curves. These results indicate that the approximations used for the calculations are quite valuable for predicting the energy distribution of partial and total DOSs in the case of Si alloys and confirms previous results reported elsewhere (Belin *et al* 1990) for other silicides.

References

Arnaud d'Avitaya F, Perio A, Oberlin J C, Campidelli Y and Chroboczek J A 1989 *Appl. Phys. Lett.* **54** 2198
Baptist R, Ferrer S, Grenet G and Poon H C 1990 *Phys. Rev. Lett.* **64** 311
Belin E, Sénémaud C, Martinage L, Veuillen J Y and Papaconstantopoulos D A 1990 *J. Phys.: Condens. Matter* **2** 3247
Gheorghiu A, Sénémaud C, Asal R and Davis E A 1995 *J. Non-Cryst. Solids* **182** 293
Hedin L and Lundqvist B J 1971 *J. Phys. C: Solid State Phys.* **4** 2064
Iandelli A, Palenzona A and Olese G L 1979 *J. Non-Common Met.* **64** 213
Keski-Rahkonen O and Krause M O 1974 *At. Data Nucl. Data Tables* **14** 139
Lerch P, Jarlborg T, Codazzi V, Loupias G and Flank A M 1992 *Phys. Rev.* B **45** 11 481
Magaud L, Julien J P and Cyrot-Lackmann F 1992a *J. Phys.: Condens. Matter* **4** 5399
Magaud L, Veuillen J Y, Lollman D, Nguyen Tan T A, Papaconstantopoulos D A and Mehl M J 1992b *Phys. Rev.* B **46** 1299
Martinage L, Pasturel A, Papaconstantopoulos D A and Cyrot-Lackmann F 1990 *Phys. Scr.* **42** 363
Scoffield J H 1976 *J. Electron Spectrosc. Relat. Phenom.* **8** 129
Sénémaud C and Ardelean I 1990 *J. Phys.: Condens. Matter* **2** 8741
Sénémaud C, Pitault B and Bourdon B 1982 *Solid State Commun.* **43** 483
Veuillen J Y, Khennou S and Nguyen Tan T A 1991a *Solid State Commun.* **79** 795
Veuillen J Y, Nguyen Tan T A, Lollman D, Guerfi N and Cinti R 1991b *Surf. Sci.* **251–2** 432